Mixture-of-Channels: Exploiting Sparse FFNs for Efficient LLMs Pre-Training and Inference

Tong Wu

Peking University wutong1109@stu.pku.edu.cn

Bin Wang

Zhejiang University 21315079@zju.edu.cn

Yutong He

Peking University yutonghe@pku.edu.cn

Kun Yuan*

Peking University kunyuan@pku.edu.cn

Abstract

Large language models (LLMs) have demonstrated remarkable success across diverse artificial intelligence tasks, driven by scaling laws that correlate model size and training data with performance improvements. However, this scaling paradigm incurs substantial memory overhead, creating significant challenges for both training and inference. While existing research has primarily addressed parameter and optimizer state memory reduction, activation memory—particularly from feed-forward networks (FFNs)—has become the critical bottleneck, especially when FlashAttention is implemented. In this work, we conduct a detailed memory profiling of LLMs and identify FFN activations as the predominant source to activation memory overhead. Motivated by this, we introduce Mixture-of-Channels (MoC), a novel FFN architecture that selectively activates only the Top-K most relevant channels per token determined by SwiGLU's native gating mechanism. MoC substantially reduces activation memory during pre-training and improves inference efficiency by reducing memory access through partial weight loading into GPU SRAM. Extensive experiments validate that MoC delivers significant memory savings and throughput gains while maintaining competitive model performance.

1 Introduction

The rise of large language models (LLMs) has marked a paradigm shift in artificial intelligence, achieving unprecedented success across natural language processing, computer vision, decision making, and coding. The key drivers behind LLMs are scaling laws [25, 39, 20], which demonstrate that model performance steadily improves with increased model size and expanded training data. However, scaling up models entails substantial memory costs, which increase training expenses, limit deployment on devices with restricted resources, and impede exploration of even larger and more capable models. Consequently, developing memory-efficient model architectures and pre-training algorithms has become crucial for continued advancement in LLMs.

1.1 Motivation

There has been extensive research on memory-efficient pre-training strategies. One prominent line of research focuses on parameter-efficient methods, which reduce the number of trainable parameters by leveraging low-rank approximations for model weights [21, 14, 27, 24, 36]. An alternative approach focuses on compressing optimizer states while maintaining the number of trainable parameters.

^{*}Corresponding author.

GaLore [61] and its variants [17, 6, 62] achieve this by leveraging low-rank gradients to compute first-and second-order moments. Adafactor [47], Adam-mini [57], and Apollo [62] reduce redundancy in the state variables of the Adam optimizer. Although these techniques improve pre-training efficiency, they do not address the memory overhead associated with activation storage. Experimental evidence [50, 13] suggests that, especially during pre-training with large batch sizes and long sequences, activation memory constitutes a substantial, often dominant, portion of the total memory footprint. This highlights the paramount importance of developing activation-efficient techniques.

In Transformer-based LLMs, activation memory primarily originates from the attention mechanism and feed-forward networks (FFNs). Significant advances such as FlashAttention [9, 8, 45] have mitigated the quadratic memory complexity $\mathcal{O}(s^2)$ of standard attention operations with respect to sequence length s, thereby reducing it to linear complexity $\mathcal{O}(s)$. This breakthrough substantially alleviates the memory overhead of attention mechanisms in long-context settings. Consequently, FFN activation memory has emerged as the dominant bottleneck, see our detailed profiling in Figure 1. However, the challenge of efficiently compressing FFN's activation memory without incurring severe performance degradation remains largely underexplored.

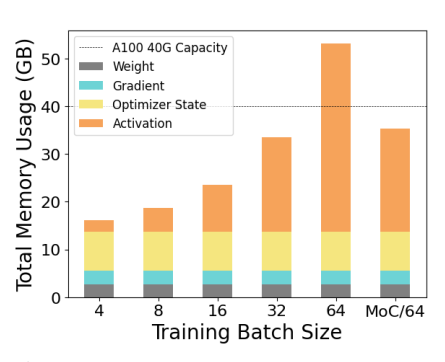


Figure 1: Memory breakdown of pretraining LLaMA-2 with a fixed sequence length of 256 and various batch size choices.

1.2 Main Results and Contributions

Mainstream LLM architectures typically employ GeLU [19] or SwiGLU [46] as the activation function in FFNs. In this work, we aim to develop activation-efficient FFN architectures tailored to such widely used activation functions, with the goal of reducing activation memory with negligible sacrifice of performance. Our main results are summarized as follows.

- **C1. Detailed activation profiling.** We provide a detailed memory profile of LLM activations with FlashAttention applied. Both theoretical analysis and empirical evidence confirm that FFN activations have become the dominant activation memory bottleneck. This finding strongly motivates the development of activation-efficient FFN architectures.
- **C2. Key activation patterns.** We analyze the value distributions of activations generated by SwiGLU functions in FFNs. Our findings show that more than 70% of activation values are near zero or slightly negative. This indicates that, for a given input token, only a small subset of activation channels are highly active and contribute meaningfully to the backward computation.
- C3. Activation-efficient FFN architecture. We propose $\underline{\mathbf{M}}$ ixture-of- $\underline{\mathbf{C}}$ hannels (MoC)—a novel FFN architecture that selectively activates only a mixture of the top-K task-relevant channels for each token. MoC leverages SwiGLU's inherent gating signal to rank channel importance. During pre-training, MoC reduces activation memory by storing only the truly-active channels; during inference, it lowers memory access overhead by loading only the required weights into GPU SRAM at each decoding step, resulting in a substantial throughput improvement.
- **C4. System-aware implementations.** We develop a set of hardware-aware kernels to further accelerate both pre-training and inference. First, we implement a batched Top-K filtering operator using the RAFT kernel library [42], achieving significant speedup over PyTorch's native implementation. Second, we design custom forward and backward kernels for the MoC architecture using Triton, delivering comparable training throughput and approximately a $1.4\times$ decoding speedup in the FFN compared to standard LLaMA-style Transformer implementations.

We conduct extensive experiments to validate the benefits of MoC. In pre-training, MoC demonstrates substantial memory savings while outperforming existing memory-efficient methods in performance. During inference, MoC achieves a 1.13× speedup in end-to-end decoding latency.

1.3 Comparison with Existing Sparse-Activation Approaches

Sparse pre-training. Recent studies have identified a distinctive property of pre-trained Transformers: their intermediate layers exhibit sparse activation patterns [58, 10, 37]. While this phenomenon has been harnessed in several post-training methods to accelerate inference [32, 48, 2], its potential for

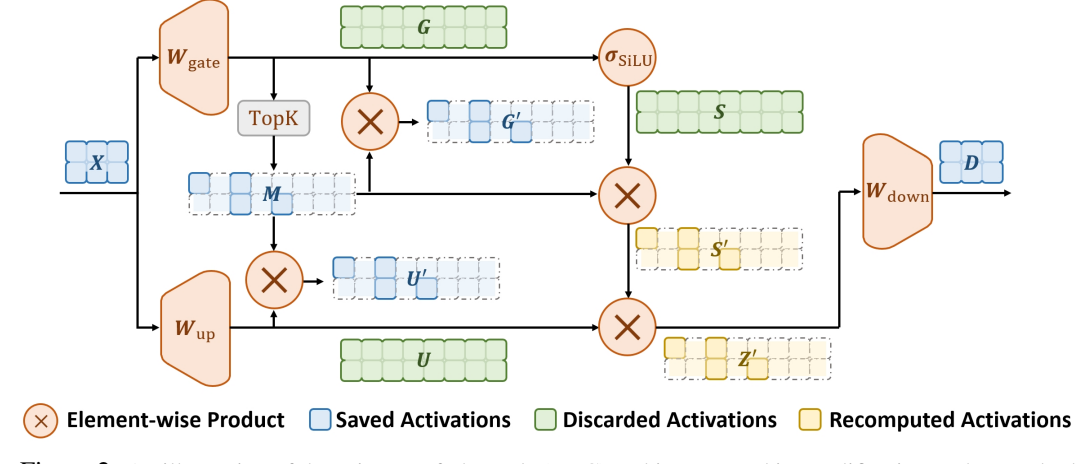


Figure 2: An illustration of the Mixture-of-channels (MoC) architecture and its modification to the standard SwiGLU FFN. The output of the gate projection is filtered by a Top-K operator. Here, U' and G' denote the sparsified versions of U and G, respectively. In MoC, components painted in blue are stored as activations during the forward pass, and those painted in yellow will be efficiently recomputed during backpropagation.

reducing activation memory during the pre-training phase remains relatively underexplored. Earlier work investigated sparse training in CNN-based architectures such as ResNet and VGG [41, 23]; however, these studies do not address sparsity patterns in LLMs. Reference [60] proposed switchable sparse-dense learning for LLM pre-training. However, this method fails to reduce peak activation memory due to its reliance on periodic dense learning phases. In contrast, our proposed MoC framework maintains persistent sparsity throughout training, thereby significantly lowering peak memory consumption. A recent effort [52] replaced the standard SwiGLU activation with SquareReLU to induce greater activation sparsity during LLM pre-training. While this modification enhances sparsity, our approach retains SwiGLU—a widely adopted activation function in LLMs—ensuring compatibility with established architectural practices.

Sparse inference. Recent advances in efficient inference for LLMs have extensively explored sparse activation patterns, primarily through two approaches: attention-based methods that dynamically manage Key-Value memory retention by selectively preserving critical pairs [54, 49, 59], and FFN-based methods that target sparsity in feed-forward networks (our work falls into this line). However, existing FFN-based approaches operate on originally dense LLMs, requiring post-training modifications [37, 52] like activation function redesign or targeted pruning to induce sparsity, while often depending on dynamic thresholding mechanisms [26, 30] whose huristic nature introduces performance variability. In contrast, our MoC FFN addresses these limitations through its intrinsic Top-K sparsity pre-training mechanism, which guarantees sparsity patterns without additional post-hoc modifications. This architectural innovation eliminates the heuristic threshold determination while simultaneously preserving both inference acceleration and model integrity.

1.4 Orthogonality to Existing Activation-Efficient Approaches

FlashAttention. FlashAttention [9, 8, 45] is an optimized attention implementation that strategically reorganizes computations to minimize memory access overhead and maximize GPU memory bandwidth utilization. Through its tiled computation and fused kernel design, it achieves significant speed improvements and memory reduction specifically within the Transformer's attention module. Our MoC architecture, in contrast, targets the memory efficiency of the FFN component, making it fundamentally orthogonal to FlashAttention. In our experiments, we combine these two techniques to deliver compounded activation efficiency gains across the entire LLM architecture.

Mixed-precision methods. Mixed-precision training has become indispensable for efficiently scaling modern LLMs, reducing memory usage and accelerating computation. The seminal work by [35] demonstrated that storing activations in FP16 enables stable training with reduced activation memory overhead. Recent studies such as GPTQ [11] and AWQ [28] have quantized activations to FP8/int4 formats in LLMs post-training with less than 1% performance degradation. To pre-train

LLMs, quantization-aware training (QAT) methods such as BitNet [51] and Quest [38] enable 4-bit quantization for activations. Mixed-precision can also be applied to our MoC structure.

Gradient checkpointing. Several system-level techniques have been proposed to improve activation memory efficiency. Gradient checkpointing [5] reduces memory consumption by selectively recomputing activations during backpropagation instead of storing them throughout the forward pass, at the cost of increased computation. Other approaches [43, 56] reduce GPU memory usage by offloading data to non-GPU resources, though this introduces additional communication overhead. Since MoC is a FFN architecture, it is compatible with gradient chekpointing.

Additional related work on parameter- and optimizer-efficient methods is discussed in Appendix A.

2 Activation Memory Profiling

This section provides a detailed analysis of activation memory during the pre-training stage of LLMs represented by LLaMA-2 [50] with FlashAttention applied.

LLM structure. Each Transformer layer consists of two main modules: Multi-Head Self-Attention (MHSA) and a Feed-Forward Network (FFN). Pre-normalization using RM-SNorm is applied before both the MHSA and FFN modules to enhance training stability. Residual connections are added after both MHSA and FFN components to facilitate the training of deep networks. The FFN module is implemented as a two-layer MLP with SwiGLU activation functions. See illustrations in Figure 3.

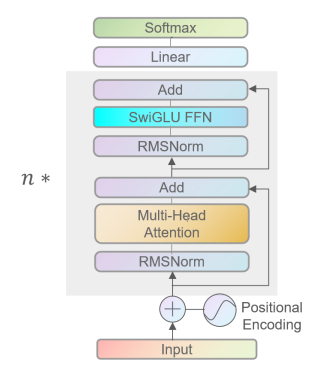


Figure 3: LLaMA-2 architecture.

Theoretical analysis. We denote the training batch size, sequence length, and model hidden dimension by b, s, and d, respectively. Let h represent the number of attention heads, define $d_h = d/h$ as the hidden dimension per head, and let $d_{\rm ffn}$ be the FFN hidden dimension. Below, we present a detailed theoretical analysis of activation memory during the pre-training phase of LLMs.

• MHSA. For each input $X \in \mathbb{R}^{s \times d}$ to the MHSA module, we first need to compute and store, for each attention head i, the following activations:

$$Q_i = XW_Q^i \in \mathbb{R}^{s \times d_h}, \quad K_i = XW_K^i \in \mathbb{R}^{s \times d_h}, \quad V_i = XW_V^i \in \mathbb{R}^{s \times d_h},$$

where $W_Q^i, W_K^i, W_V^i \in \mathbb{R}^{d \times d_h}$ are weights for the *i*-th attention head. We next store

$$A_i = \text{FlashAttention}(Q_i, K_i, V_i) \in \mathbb{R}^{s \times d_h}$$
 and $O = AW_o \in \mathbb{R}^{s \times d}$,

where $A=[A_1;\cdots;A_h]\in\mathbb{R}^{s\times d}$ is the concatenated attention output and $W_o\in\mathbb{R}^{d\times d}$ is the weight. Since FlashAttention leverages kernel fusion and recomputation techniques, it eliminates the need to store intermediate variables such as attention weights or softmax outputs during the forward pass. As a result, MHSA needs to store Q,K,V,A and O, amounting to a total of 5sd activations. For a batch size of b, this corresponds to an activation memory footprint of 5bsd.

• FFN. For each input $X \in \mathbb{R}^{s \times d}$ to the FFN module, we first compute and store:

$$G = XW_{\text{gate}} \in \mathbb{R}^{s \times d_{\text{fin}}}, \quad U = XW_{\text{up}} \in \mathbb{R}^{s \times d_{\text{fin}}},$$
 (1)

where $W_{\rm gate}, W_{\rm up} \in \mathbb{R}^{d \times d_{\rm fin}}$ are the weights corresponding to the gating and up-sampling branches in the SwiGLU activation. We then compute and store

$$S = \text{SiLU}(G) \in \mathbb{R}^{s \times d_{\text{fin}}}, \quad Z = S \odot U \in \mathbb{R}^{s \times d_{\text{fin}}}, \quad D = ZW_{\text{down}} \in \mathbb{R}^{s \times d},$$
 (2)

where $W_{\mathrm{down}} \in \mathbb{R}^{d_{\mathrm{fin}} \times d}$ is the down-sampling weight. As a result, the FFN module needs to store U, G, S, Z and D, amounting to a total of $(4d_{\mathrm{ffn}} + d)s$ activations. For a batch size of b, this corresponds to an activation memory footprint of $b(4d_{\mathrm{ffn}} + d)s$. Since the typical choice of d_{ffn} is $\frac{8d}{3}$, the activation memory is around 11.67bsd.

• **RMSNorm.** For each row $x \in \mathbb{R}^d$ of the input $X \in \mathbb{R}^{s \times d}$, we compute and store $y = \frac{x}{\text{RMS}(x)} \odot g \in \mathbb{R}^d$ where $\text{RMS}(x) = (\frac{1}{d} \sum_{i=1}^d x_i^2 + \epsilon)^{1/2}$ and and $g \in \mathbb{R}^d$ is a learned weight

vector. Since there are s rows in total, this results in sd activations per RMSNorm layer. As there are two RMSNorm layers—one before the MHSA module and one before the FFN module—the total number of activations is 2sd. For a batch size of b, the activation memory is 2bsd.

• Residual connections. Each residual connection adds the module output to its input. Given input $X \in \mathbb{R}^{s \times d}$, we compute $Z = X + Y \in \mathbb{R}^{s \times d}$, where Y is the module output. To support backpropagation, the input X must be stored, requiring sd activations. Since each transformer layer has two residual connections, the total is 2bsd activations.

Following the above analysis, we finally decompose the activation memory into

 $Layer\ Activation = Attention\ 5bsd + FFN\ 11.67bsd + RMSNorm\ 2bsd + Residual\ 2bsd$

This shows that the FFN dominates activation memory when FlashAttention is applied. Moreover, FFNs primarily consist of large matrix multiplications, which are difficult to optimize without compromising model performance.

Empirical profiling. The right table presents profiling when batchsize is 64 and sequence length is 256. In both models, the FFN-to-Attention memory ratio is approximately 2.3, which closely matches our theoretical analysis.

		LLaMA (350M)	LLaMA (1.3B)
Per- Layer (×24)	Attention FFN Others	177M 400M 68M	336M 791M 134M
LL	M head	2.16G	2.16G
7	Fotal	17.64G	32.4G

3 The Mixture-of-Channels Architecture

We introduce <u>Mixture-of-Channels</u> (MoC), an activation-efficient FFN architecture designed to substantially reduce memory usage during pre-training and accelerate decoding during inference.

3.1 SiLU Activation Pattern.

SiLU (also known as Swish₁) is an activation function commonly used in the FFN layers of LLMs, see (1) and (2). SiLU is defined as

$$SiLU(x) = \frac{x}{1 + \exp(-x)},$$
(3)

which is illustrated in Figure 4. Notably, when $x \ge 0$, $\mathrm{SiLU}(x)$ approaches x, indicating strong activation; conversely, for negative x, the output tends toward zero, implying that the input is largely suppressed. This nonlinear behavior naturally induces a degree of

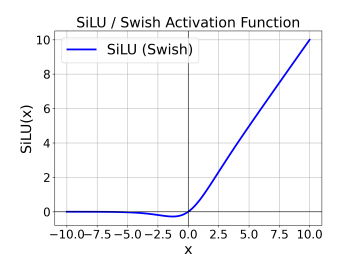


Figure 4: SiLU activation.

sparsity in the FFN outputs. Motivated by this observation, we investigate how many channels remain active after applying SiLU in pre-trained LLMs.

Figure 5 presents histograms of pre-SiLU and post-SiLU activations from various layers of the pre-trained LLaMA-2 model. As shown in Figures 5a–5c, approximately 70% of the inputs to the SiLU function are negative. Based on the SiLU expression illustrated in Figure 4, this results in about 70% of the SiLU outputs being close to zero (see Figures 5d–5f). This implies that a significant portion of the channels are effectively suppressed after SiLU activation, with only around 30% remaining active. This key observation motivates the design of activation-efficient FFN architectures. Similar observations also hold for MoE models, see the results in Section 6.

3.2 Mixture-of-Channels Architecture

Recalling the FFN structure listed in (1)–(2), for input $X \in \mathbb{R}^{s \times d}$, we first compute

$$G = XW_{\text{gate}}, \qquad U = XW_{\text{up}}.$$
 (4)

According to the SiLU activation pattern in Section 3.1, most elements in G are negative and are suppressed by the SiLU activation function. To reduce activation memory, we propose retaining

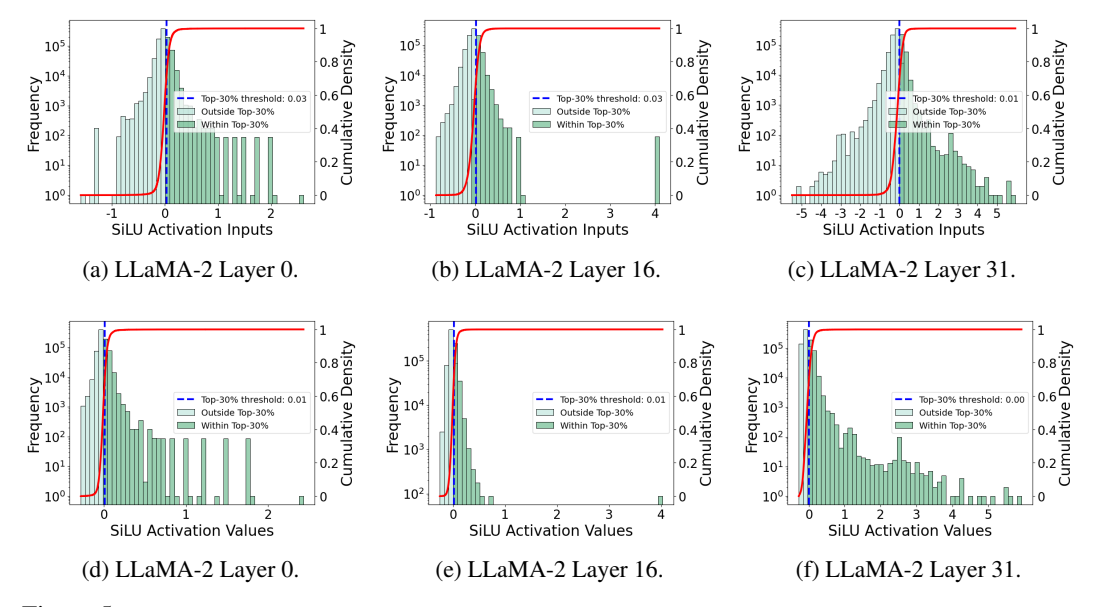


Figure 5: Histograms of pre-SiLU and post-SiLU activations from different layers of LLaMA-2. Subfigures (a), (b), and (c) correspond to the pre-SiLU activations, while subfigures (d), (e), and (f) show the post-SiLU activations. The blue dashed line marks the threshold for the top 30% of activations by value, and the red curve represents the cumulative distribution.

only the large positive elements of G and masking out the rest during pre-training. To this end, we introduce a binary mask matrix $M = \text{TopK}(G) \in \mathbb{R}^{s \times d_{\text{ffn}}}$, in which the entries of M satisfy:

$$M_{ij} = \begin{cases} 1, & \text{if } G_{ij} \text{ is among the top-} K \text{ largest values in row } i \text{ of } G, \\ 0, & \text{otherwise.} \end{cases}$$
 (5)

Here, the top-K selection is applied in a row-wise manner, so each row of M contains exactly K ones. Note that M retains the top-K largest values (not the largest in absolute value), focusing on strongly active channels in each row of G. We then apply the mask matrix M to sparsify the intermediate representations S and Z in equation (2) as follows:

$$S = \text{SiLU}(G), \quad S' = S \odot M, \quad Z' = S' \odot U, \quad D = Z'W_{\text{down}}.$$
 (6)

This completes the formulation of the proposed architecture. Since it selectively utilizes a mixture (not all) of the channels from the original \bar{S} and Z matrices, we refer to it as the Mixture-of-Channels (MoC) architecture. Figure 2 illustrates the MoC architecture and its forward process.

Activation-Efficient Pre-Training with Mixture-of-Channels

Backward propagation. We now derive the backward propagation step for the MoC architecture. Let ∇_D denote the gradient of the loss with respect to the output D. The backward propagation is:

$$\nabla_{W_{\text{down}}} = (Z')^{\top} \nabla_{D}, \qquad \nabla_{Z'} = \nabla_{D} W_{\text{down}}^{\top}, \qquad (7a)$$

$$\nabla_{S'} = (U \odot M) \odot \nabla_{Z'}, \qquad \nabla_{U} = S' \odot \nabla_{Z'}, \qquad (7b)$$

$$\nabla_{S} = \nabla_{S'}, \qquad \nabla_{G} = \nabla_{S'} \odot (\nabla \text{SiLU})(G), \qquad (7c)$$

$$\nabla_{S'} = (U \odot M) \odot \nabla_{Z'}, \qquad \nabla_U = S' \odot \nabla_{Z'}, \tag{7b}$$

$$\nabla_S = \nabla_{S'}, \qquad \qquad \nabla_G = \nabla_{S'} \odot (\nabla \text{SiLU})(G),$$
 (7c)

$$\nabla_{S} = \nabla_{S'}, \qquad \nabla_{G} = \nabla_{S'} \odot (\nabla \text{SiLU})(G), \qquad (7c)$$

$$\nabla_{W_{\text{gate}}} = X^{\top} \nabla_{G}, \qquad \nabla_{W_{\text{up}}} = X^{\top} \nabla_{U}, \qquad (7d)$$

$$\nabla_X = \nabla_G W_{\text{gate}}^\top + \nabla_U W_{\text{up}}^\top, \tag{7e}$$

where $\nabla \text{SiLU}(\cdot)$ in (7c) is the gradient operator of the SiLU activation function defined in (3). To facilitate the backward propagation steps described above, we need to store the activations $Z' = S' \odot U = S \odot M \odot U = Z \odot M$ from (7a), as well as $U \odot M$ and $S' = S \odot M$ from (7b). Moreover, since $\nabla_{S'} = \nabla_S = U \odot M \odot \nabla_{Z'}$ exhibits a sparse pattern, it suffices to store only $G \odot M$ in (7c) instead of the full matrix G. Table 1 compares the activation memory of the standard

FFN and the MoC architecture, where each row of M retains the top 20% of its elements, as used in our experiments. When set $d_{\rm ffn}=\frac{8d}{3}$, MoC substantially reduces activation memory usage from 11.67bsd to 3.67bsd, making the FFN activation even smaller than that of FlashAttention.

MoC + GCP. Recall from (2) that $S = \mathrm{SiLU}(G)$ and $Z = S \odot U$, both of which involve inexpensive element-wise operations. As a result, it is unnecessary to store S and S in memory; instead, they can be recomputed from S during backpropagation. This technique is known as gradient checkpointing (GCP). Table 1 compares the activation memory and additional computation overhead introduced by gradient checkpointing (GCP) for the standard FFN and the MoC architecture. MoC+GCP achieves substantial memory savings with significantly lower computational overhead compared to FFN+GCP.

Table 1: Activation memory comparison during pre-training. "GCP Comp" refers to computational overhead introduced by gradient checkpointing. Memory values in parentheses are computed using $d_{\text{ffn}} = \frac{8d}{3}$.

	MoC	MoC+GCP	FFN	FFN+GCP
	$G\odot M$	$G\odot M$	G	G
Stored	$U\odot M$	$U\odot M$	U	U
Activations	$S\odot M$	_	S	_
Activations	$Z\odot M$	_	Z	_
	${\cal M}$ and ${\cal D}$	M and D	D	D
Memory	$bsd_{\mathrm{ffn}} + bsd$	$0.6bsd_{\mathrm{ffn}} + bsd$	$4bsd_{\mathrm{ffn}} + bsd$	$2bsd_{\mathrm{ffn}} + bsd$
Cost	(3.67bsd)	(2.6bsd)	(11.67bsd)	(6.33bsd)
CCD Comp		$0.4bsd_{\mathrm{ffn}}$		$2bsd_{\mathrm{ffn}}$
GCP Comp.	_	(1.07bsd)	_	(5.33bsd)

MoC's Expressive Power. To quantify the expressive capacity of MoC despite its efficiency-oriented design, we analyze its relationship to the standard FFN introduced in Section 2. Let $\mathcal{H}_{d_{\mathrm{ffn}}}$ denote the class of operators $\mathbb{R}^d \to \mathbb{R}^d$ implemented by a standard FFN with hidden dimension d_{ffn} , and let $\mathcal{H}_{d_{\mathrm{moc}}}^{a:b}$ denote the class of operators $\mathbb{R}^d \to \mathbb{R}^d$ realized by an $\mathrm{MoC}_{a:b}$ model (where $b \mid d_{\mathrm{moc}}$ and $a \leq b$) with hidden dimension d_{moc} . Here, a:b denotes the configuration of MoC's Grouped Top-K selection strategy, in which a elements are selected from each contiguous group of b entries. We establish the following theorem.

Theorem 1. For all $a \leq b$ and $d_{ffn} \in \mathbb{N}^*$, it holds that (Proof is in Appendix B)

$$\mathcal{H}_{d_{\mathrm{ffn}}} \subseteq \mathcal{H}_{d_{\mathrm{moc}}}^{a:b}, \quad \textit{where} \quad d_{\mathrm{moc}} = b \lceil d_{\mathrm{ffn}}/a \rceil.$$

Remark. Theorem 1 provides a lower bound on MoC's expressive capacity. In particular, when $b/a = \Theta(1)$, any standard FFN can be emulated by an MoC_{a:b} model with only a constant-factor increase in parameters. Hence, MoC_{a:b} matches the expressive power of a standard FFN up to constant factors in model size.

Hardware-aware implementation. While the MoC architecture theoretically provides computation savings, realizing this benefit in practice requires careful system-level optimization. In particular, unstructured sparsity does not translate to actual computational gains on modern accelerators (e.g., GPUs and TPUs), as they are not designed to exploit irregular sparsity patterns efficiently. Additionally, the top-K selection

	Standard FFN (ms)	MoC using optimized kernels (ms)
Forward	20.2	21.1
Backward	21.6	22.8
Total	41.8	43.9

introduces computational overhead, potentially offsetting the theoretical advantages. We made two efforts to address these issues:

- Customized MoC kernels. We develop a hardware-aware implementation by customizing a batched top-K operator using the RAFT library [42] and designing fused Triton kernels to accelerate intermediate computations. These optimizations enable MoC to achieve computation efficiency comparable to that of standard FFNs, see the above tables.
- MoC with structured 2:8 sparsity. We implement structured 2:8 sparsity—where only 2 out of every 8 consecutive weights are retained—a format natively supported by NVIDIA Ampere

Table 2: Comparison of different memory-efficient algorithms during the pre-training of various LLaMA-based Transformer models on the C4 dataset. We report validation perplexity alongside total memory usage, which includes model weights, gradients, optimizer states, and activations. Perplexity results for GaLore and SLTrain are taken from [61, 14]. Constant K is the number of activated channels. We typically set $K = 0.5 d_{\rm model}$, which is 18.75% of of the channel dimension $d_{\rm ffn} = 8 d_{\rm model}/3$.

	60M	130M	350M	1B
FFN-based LLM + AdamW	30.44 (38.3G)	23.92 (54.1G)	18.26 (52.5G)	15.56 (56.6G)
GaLore	34.88 (38.1G)	25.36 (53.9G)	18.95 (51.7G)	15.64 (52.5G)
SLTrain	34.15 (33.6G)	26.04 (59.4G)	19.42 (69.1G)	16.14 (70.0G)
MoC	30.59 (21.8G)	24.02 (41.7G)	18.57 (34.6G)	15.80 (41.9G)
MoC _{2:8}	31.02 (22.1G)	24.12 (42.3G)	18.68(36.4G)	15.62 (42.7G)
batch size per GPU $K/d_{ m model}$ Training Tokens	256	256	128	64
	128 / 256	384 / 768	512 / 1024	1024 / 2048
	1.1B	2.2B	6.4B	13.1B

Table 3: Zero-shot evaluation results on downstream tasks.

	MMLU	ARC-Easy	ARC-Challenge	PIQA	TruthfulQA-MC2	Avg.
LLaMA-1B	0.231	0.426	0.237	0.678	0.398	0.394
MoC-1B	0.230	0.416	0.237	0.636	0.455	0.395
$MoC_{2:8}$ -1B	0.230	0.432	0.242	0.655	0.454	0.403

and Hopper architectures. This structured sparsity unlocks the computational efficiency of MoC on compatible hardware, bridging the gap between theoretical and practical performance. We denote $MoC_{2:8}$ as the MoC architecture supports structured 2:8 sparsity.

5 Accelerated Inference with Mixture-of-Channels

Now we consider the inference process with MoC architecture. Given an input token $x \in \mathbb{R}^{1 \times d}$, the MoC inference will proceed as follows.

- (Linear projection) Compute $g = xW_{\text{gate}} \in \mathbb{R}^{1 \times d_{\text{ffn}}}$ and $u = xW_{\text{up}} \in \mathbb{R}^{1 \times d_{\text{ffn}}}$.
- (Top-K masking) Construct a binary mask $m \in \{0,1\}^{1 \times d_{\mathrm{ffn}}},$ where:

$$m_j = \begin{cases} 1, & \text{if } g_j \text{ is among the top-} K \text{ values in } g, \\ 0, & \text{otherwise.} \end{cases}$$

- (Nonlinearity and sparsification) Compute $s = \mathrm{SiLU}(g), s' = s \odot m, z' = s' \odot u.$
- (Final output) Compute the output $d=z'W_{\mathrm{down}}=\sum_{j\in\mathcal{C}}z'_jw_j\in\mathbb{R}^{1\times d}$ where w_j denotes the j-th row of W_{down} , and \mathcal{C} is the set of active (i.e., unmasked) channels.

It is observed that the inference relies only on the subset of active channels selected per token; this selection is driven by SwiGLU's native gating mechanism, which identifies the top-K most relevant channels for each input token.

Accelerated inference via sparse activation. The decoding latency of LLMs is primarily IO-bounded by loading weights from GPU HBM to SRAM, and our sparse MoC architecture delivers substantial inference-time speedups by alleviating unnecessary memory access costs (MACs). In a standard FFN with hidden dimension $d_{\rm ffn}$, each token incurs two dense projections ($xW_{\rm gate}$ and $xW_{\rm up}$) plus one down-projection ($zW_{\rm down}$), for a total of $2d\times d_{\rm ffn}+d_{\rm ffn}\times d=3\,d\,d_{\rm ffn}$ MACs per token. By contrast, MoC retains only the top-K channels in each of u and z', so we need only K columns of $W_{\rm up}$ and K rows of $W_{\rm down}$, yielding $d\,d_{\rm ffn}+2\,K\,d$ MACs per token. When $K\ll d_{\rm ffn}$, this represents an $\mathcal{O}(K/d_{\rm ffn})$ reduction in MACs, contributing to much faster inference.

Intrinsic sparse pattern. One notable advantage of the MoC architecture is that it naturally introduces an intrinsic sparsity pattern during pre-training, as only the top-K channels are activated for each

Table 4: Validation perplexity and memory consumption of pre-training GQA models on the C4 dataset.

Model	Structure	Perplexity	Memory (GB)
LLaMA-130M	GQA	24.02	53.9
LLaMA-130M	GQA+MoC	24.26	34.4
LLaMA-350M	GQA	18.51	52.9
LLaMA-350M	GQA+MoC	18.69	36.9

Table 5: Validation perplexity of pre-training on the C4 dataset.

Model	Perplexity
Qwen3-300M	18.52
Qwen3-300M+MoC	18.59
LLaMA-7B	26.14
LLaMA-7B+MoC	26.47

input. In contrast, existing sparse inference methods built on dense LLMs typically require post-hoc pruning or distillation to achieve comparable efficiency [54, 49, 59, 37, 52, 26, 30], which can degrade performance or necessitate additional training steps.

6 Experiments

We evaluate the pre-training performance and inference efficiency of LLMs using the MoC architecture. All experiments are conducted on NVIDIA A800 GPUs with 80 GB of VRAM.

6.1 Memory Reduction and Training Performance

Pre-training LLaMA on C4. To evaluate the expressive power of models using the MoC architecture, we pre-train LLaMA-based large language models with various memory-efficient strategies on the C4 dataset [40]. We closely follow the experimental setup in GaLore [61] to ensure fair comparisons with several baselines, including vanilla AdamW applied to standard FFN-based LLMs, GaLore [61], which aims to reduce optimizer memory usage, and SLTrain [14], which focuses on reducing weight memory. Our evaluation considers both model performance and pre-training memory consumption. All models are trained using the AdamW [33] optimizer with a cosine annealing learning rate scheduler, with all other hyperparameters aligned to those of the baseline methods. FlashAttention is enabled, activation checkpointing is disabled, and the BF16 data format is employed. Additional experimental details are provided in Appendix C. (**Performance and Memory**) The training results are presented in Table 2. Both MoC and MoC_{2:8} achieve the best performance among all baselines while significantly reducing memory consumption by substantially reducing activations—the dominant contributor to overall memory usage. (Throughput) We measure the throughput of different models by pre-training LLaMA-350M and LLaMA-1B using batch sizes of 128 and 64, respectively, on a single NVIDIA A800 GPU. The results in Appendix C demonstrates that MoC achieves training efficiency comparable to that of the vanilla LLaMA model due to our hardware-aware kernel implementation.

6.2 Generalization and Applicability

Downstream evaluations. To thoroughly assess the generalization capabilities of MoC models, we use the lm-evaluation-harness framework [12] to evaluate their zero-shot performance across a range of NLP benchmarks. This standardized suite ensures reproducibility and enables consistent, reliable comparisons of model performance. Specifically, we select five representative tasks across four categories:

• Natural language understanding: MMLU [18]

Table 6: Comparison of Mixtral with MoC-style FFN or vanilla FFN on the C4 dataset. We report validation perplexity alongside total memory usage, which includes model weights, gradients, optimizer states, and activations. Constant K is the number of activated channels. We typically set $K=0.5d_{\rm model}$, which is 18.75% of of the channel dimension $d_{\rm ffn}=8d_{\rm model}/3$.

_	160M	530M
Vanilla Mixtral Mixtral+MoC	23.77 (48.3G) 24.44 (38.2G)	18.65 (41.7G) 18.88 (30.0G)
batch size per GPU $K/d_{ m model}$	256 256 / 512	128 512 / 1024

Table 7: Inference latency(μ s) of a single FFN layer for a single batch size at each decoding step.

	Gate Proj.	Up&Down Proj.	Top-K	Other	Total	Rel. Speedup
Standard FFN	24	56.5	0	4.8	85.3	1.0×
MoC	24	18.2	15	4.6	61.8	1.38×

Table 8: End-to-end inference speedup, measured by decoding throughput.

	Decode Latency	Decode Throughput	Rel. Speedup
Vanilla LLaMA	4.75 ms	210.45 tokens/sec	1.0×
MoC	4.20 ms	238.10 tokens/sec	1.13×

• **Reasoning:** ARC-Easy and ARC-Challenge [7]

• Commonsense understanding: PIQA [4]

• Truthfulness: TruthfulQA [29]

As shown in Table 3, our model demonstrates strong performance across a broad range of tasks relative to the baseline LLaMA model. However, a modest performance gap persists in specific benchmarks such as PIQA [4], suggesting limitations in commonsense reasoning capabilities.

Applicability to additional base models. To further assess the generalization of MoC across different model architectures and scales, we extend our study to LLaMA with Grouped Query Attention (GQA) [1], Qwen3 [55], and LLaMA-7B. As summarized in Tables 4 and 5, MoC demonstrates strong compatibility with these settings: it consistently preserves model performance while substantially reducing memory consumption. These results suggest that MoC is broadly applicable to modern LLM architectures beyond the standard LLaMA baseline.

Compatibility with MoE architectures. To further investigate activation sparsity in MoE models and demonstrate that MoC offers activation efficiency orthogonal to the MoE architecture, we pre-train the Mixtral model [22]—a representative MoE-based large language model—on the C4 dataset and evaluate its perplexity on a held-out test set. Specifically, for the Mixtral+MoC variant, we replace each expert's MLP with a MoC-style feedforward network and compare its performance to the baseline after pre-training. We adopt an experimental setup consistent with that described in Appendix C, with full configurations detailed in Table 20. As shown in Table 6, Mixtral with MoC achieves comparable perplexity to the original model while significantly reducing memory consumption, confirming the viability of MoC within MoE architectures.

6.3 Inference Acceleration

FFN inference speedup. We measure the latency of a single FFN layer in LLaMA-1.3B for a batch size of one at each decoding step, with results reported in Table 7. To ensure a fair comparison with the vanilla FFN, both implementations are optimized using torch.compile(). As discussed earlier, MoC leverages the sparsity pattern in SiLU activations, which significantly accelerates both

Table 9: Training throughput (samples/sec) on a single NVIDIA A800 GPU.

Model + Optimizer	350M	1B
LLaMA (AdamW)	28 830	5 975
LLaMA (GaLore + AdamW)	24 645	5771
MoC (AdamW)	27 954	5 806
batch size	128	64

Table 10: Inference latency(μ s) of a single FFN layer for a single batch size at each decoding step.

	Gate Proj.	Up&Down Proj.	Top-K	Other	Total	Rel. Speedup
Standard FFN	24	56.5	0	4.8	85.3	1.0×
MoC MoC _{2:8}	24 24	18.2 18	15 9.4	4.6 4.6	61.8 56.0	1.38× 1.52×

Table 11: Inference latency (μ s) of a single FFN layer across different batch sizes.

Batch Size	Dense FFN	MoC	Relative Acceleration
1	316	191	1.65×
2	360	227	1.59×
3	360	227	1.59×
4	357	230	1.55×

the up-projection and down-projection computations. This effectively offsets the overhead introduced by the top-K selection. Table 7 shows that MoC achieves $1.38\times$ speedup compared to FFN.

End-to-end inference speedup. We also measure the end-to-end decoding throughput of LLaMA 1.3B and MoC 1.3B, with results reported in Table 8. The input batch size is 1, and the prompt and generation length are 128. Both models are optimized using torch.compile().

MoC with 2:8 sparsity. In Section 5, we propose MoC with 2:8 sparsity, which retains only the top-2 outputs among every 8 activations. As shown in Tables 2, 3, and 9, $MoC_{2:8}$ achieves training efficiency and performance comparable to denser variants and vanilla LLaMA. Furthermore, according to the decoding latency of the FFN reported in Table 10, $MoC_{2:8}$ offers superior inference performance by aligning with the coalesced memory access patterns of GPU hardware. Notably, we hypothesize that $MoC_{2:8}$ can accelerate pre-training by leveraging the accelerated semi-sparse GEMM support available on recent NVIDIA GPUs, thanks to its sparse activation patterns. A thorough investigation of this potential remains beyond the scope of this study due to time constraints and is left for future work.

Batch size scaling. We further investigate the inference-time acceleration of MoC under different batch sizes. As shown in Table 11, MoC consistently delivers substantial latency reductions compared to the dense baseline, even as the batch size increases from 1 to 4. These results demonstrate that the benefits of activation sparsity are not confined to the single-token decoding case, but also extend to small-batch scenarios that are common in practical auto-regressive inference.

Implementation discussion. From an implementation perspective, modern GPUs (e.g., NVIDIA architectures) comprise hundreds of independent Streaming Multiprocessors (SMs), each equipped with dedicated on-chip memory. During inference, different sequences within a batch can be dispatched to separate SMs, enabling each SM to load only the relevant (sparse) portions of the weight matrices. This strategy preserves sparsity, avoids redundant memory transfers, and underpins MoC's ability to sustain acceleration at small but non-trivial batch sizes.

Table 12: Validation perplexity of LLaMA-based Transformer models pre-trained on the C4 dataset.

Model Size	dReLU [48]	ReLU	MoC
130M	26.34	28.98	24.02
350M	20.09	19.07	18.57

Table 13: Validation perplexity of LLaMA-based Transformer models pre-trained on the C4 dataset.

Model Size	BackRazor	MoC
130M	25.12	24.02
350M	19.40	18.57
1B	16.97	15.62

Table 14: Peak memory consumption and throughput comparison between MoC and pure GCP.

Method	Peak Memory (GB)	Throughput (tokens/s)
FFN+GCP	39.43	6160
MoC+GCP	41.90	7470

Table 15: Effect of top-*K*'s position on validation perplexity of different model sizes.

Top- K Position	MoC-60M	MoC-130M	
Before SiLU	30.59	24.02	
After SiLU	30.92	25.45	

Table 16: Effect of number of activated channels K on MoC-130M's validation perplexity.

# Activated Channels K	Perplexity
256	25.65
384	24.02
512	23.91

6.4 Comparisons with Related Approaches

Comparisons with ReLU and dReLU. To further demonstrate the effectiveness of MoC, we extend our comparisons to several other sparsity-based baseline methods, including Top-K gating with dReLU [48] and standard ReLU activations. As shown in Table 12, both dReLU and ReLU lead to noticeable performance degradation, whereas MoC consistently achieves lower validation perplexity. This highlights the importance of MoC's design in preserving the representational capacity of the original architecture while introducing sparsity.

Comparison with BackRazor. We further compare MoC against BackRazor [23], a memory-efficient pre-training algorithm that leverages a Top-K sparsifier to compress activations stored for backpropagation. As shown in Table 13, MoC consistently outperforms BackRazor across different model scales (130M, 350M, and 1B parameters) on the C4 dataset. These results highlight that MoC not only provides substantial memory savings but also better preserves the model's representation ability during training.

Comparison with gradient checkpointing. To further highlight MoC's advantage in the memory–compute trade-off, we compare it against the pure gradient checkpointing (GCP) method. As discussed in Section 4, MoC already incorporates gradient checkpointing for selected activations; therefore, we denote it as MoC+GCP in this subsection. As shown in Table 14, when FFN+GCP and MoC+GCP exhibit comparable peak memory consumption, their throughput differs substantially: FFN+GCP achieves 6160 tokens/s, whereas MoC+GCP reaches 7470 tokens/s. This result demonstrates that MoC+GCP preserves memory efficiency while avoiding the severe throughput degradation inherent in pure recomputation-based approaches.

Table 17: Validation perplexity of MoC-350M pre-trained on the C4 dataset with different K values.

\overline{K}	Memory (GB)	Perplexity
256	29.2	18.79
512	34.6	18.57
768	39.9	18.52
1024	52.5	18.26

Table 18: Training throughput and GPU memory usage for pre-training LLaMA-1B on a single NVIDIA A800 (80GB) GPU. "bsz" denotes batch size, and "OOM" stands for out-of-memory.

	LLaMA, bsz=64	LLaMA, bsz=128	MoC, bsz=64	MoC, bsz=128
Training Throughput (tokens/s)	7639	OOM	7470	7714
GPU Memory Usage (GB)	56.6	OOM	41.9	73.7

6.5 Ablation and Analysis

Effect of top-K **position.** In Table 15, we evaluate the performance of MoC-60M and MoC-130M by applying the top-K operator either before or after the SiLU activation function. The results indicate that placing the top-K operator before the activation generally yields better performance.

Effect of the number of channels K. We study how the number of activated channels K affects MoC. A larger K generally improves representational capacity and reduces perplexity, whereas a smaller K yields higher sparsity, leading to greater memory savings and faster inference. Thus, choosing K involves balancing performance and efficiency. To guide our setup, we conduct ablation experiments on different K values with MoC-130M (Table 16) and MoC-350M (Table 17). The results confirm that performance improves as K increases, but memory usage grows roughly linearly with K. Considering this trade-off, we adopt K=512 for MoC-350M in our main experiments.

Efficiency gains from reduced memory cost. The memory reduction offered by MoC can translate into practical training efficiency gains. In particular, smaller memory footprints allow for larger batch sizes on the same hardware, which may improve throughput by reducing communication and synchronization overhead. As shown in Table 18, MoC enables pre-training LLaMA-1B with a batch size of 128 on a single NVIDIA A800 (80GB) GPU, a setting that vanilla LLaMA cannot support due to out-of-memory (OOM) errors. With this enlarged batch size, MoC achieves a training throughput of 7714 tokens/s, surpassing vanilla LLaMA's 7639 tokens/s. This demonstrates that MoC not only reduces memory consumption but can also unlock additional efficiency benefits during large-scale pre-training.

Sparsity Patterns in MoE Models. We observe that sparse activation is a widespread phenomenon in large language models, not limited to LLaMA-like architectures. To illustrate this, Figure 6 presents histograms of pre-SiLU and post-SiLU activations from various layers of LLaMA-MoE [63], a pre-trained MoE model. The activations in LLaMA-MoE exhibit significant sparsity, closely resembling the patterns observed in LLaMA, as discussed in Section 3.1.

7 Conclusion and Limitations

We propose Mixture-of-Channels (MoC), a novel feedforward network (FFN) architecture that activates only the Top-K most relevant channels per token, guided by the native gating mechanism of SwiGLU. MoC significantly reduces activation memory during pre-training and improves inference efficiency by reducing memory access costs through selective channel activation. One limitation of MoC is that it has not yet been evaluated in conjunction with Mixture-of-Experts (MoE) architectures, where interactions between MoC's fine-grained channel sparsity and expert-level sparsity remain an open question for future exploration.

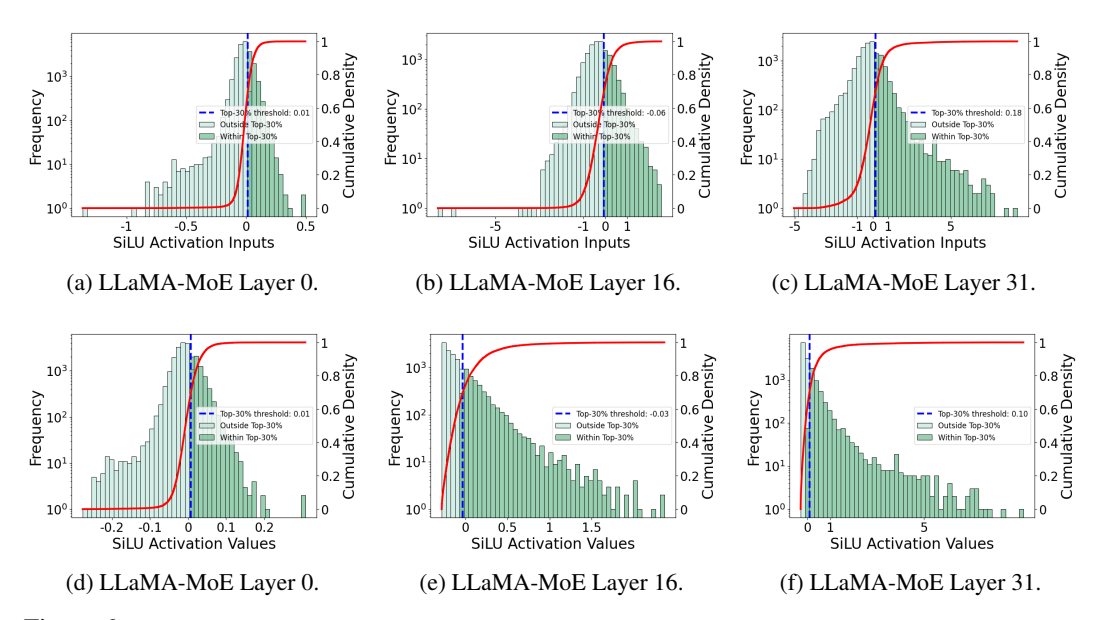


Figure 6: Histograms of pre-SiLU and post-SiLU activations from different layers of LLaMA-MoE [63]. Subfigures (a), (b), and (c) correspond to the pre-SiLU activations, while subfigures (d), (e), and (f) show the post-SiLU activations. The blue dashed line marks the threshold for the top 30% of activations by value, and the red curve represents the cumulative distribution.

References

- [1] J. Ainslie, J. Lee-Thorp, M. De Jong, Y. Zemlyanskiy, F. Lebrón, and S. Sanghai. Gqa: Training generalized multi-query transformer models from multi-head checkpoints. *arXiv* preprint arXiv:2305.13245, 2023.
- [2] K. Alizadeh, S. I. Mirzadeh, D. Belenko, S. Khatamifard, M. Cho, C. C. Del Mundo, M. Rastegari, and M. Farajtabar. Llm in a flash: Efficient large language model inference with limited memory. In *Proceedings of the 62nd Annual Meeting of the Association for Computational Linguistics (Volume 1: Long Papers)*, pages 12562–12584, 2024.
- [3] D. Biderman, J. Portes, J. J. G. Ortiz, M. Paul, P. Greengard, C. Jennings, D. King, S. Havens, V. Chiley, J. Frankle, et al. Lora learns less and forgets less. arXiv preprint arXiv:2405.09673, 2024.
- [4] Y. Bisk, R. Zellers, R. L. Bras, J. Gao, and Y. Choi. Piqa: Reasoning about physical commonsense in natural language. In *Thirty-Fourth AAAI Conference on Artificial Intelligence*, 2020.
- [5] T. Chen, B. Xu, C. Zhang, and C. Guestrin. Training deep nets with sublinear memory cost. *arXiv preprint arXiv:1604.06174*, 2016.
- [6] X. Chen, K. Feng, C. Li, X. Lai, X. Yue, Y. Yuan, and G. Wang. Fira: Can we achieve full-rank training of llms under low-rank constraint? *arXiv preprint arXiv:2410.01623*, 2024.
- [7] P. Clark, I. Cowhey, O. Etzioni, T. Khot, A. Sabharwal, C. Schoenick, and O. Tafjord. Think you have solved question answering? try arc, the ai2 reasoning challenge. *arXiv:1803.05457v1*, 2018.
- [8] T. Dao. Flashattention-2: Faster attention with better parallelism and work partitioning. *arXiv* preprint *arXiv*:2307.08691, 2023.
- [9] T. Dao, D. Fu, S. Ermon, A. Rudra, and C. Ré. Flashattention: Fast and memory-efficient exact attention with io-awareness. *Advances in neural information processing systems*, 35:16344–16359, 2022.
- [10] H. Dong, B. Chen, and Y. Chi. Towards structured sparsity in transformers for efficient inference. In Workshop on Efficient Systems for Foundation Models@ ICML2023, 2023.
- [11] E. Frantar, S. Ashkboos, T. Hoefler, and D. Alistarh. Gptq: Accurate post-training quantization for generative pre-trained transformers. *arXiv* preprint *arXiv*:2210.17323, 2022.
- [12] L. Gao, J. Tow, B. Abbasi, S. Biderman, S. Black, A. DiPofi, C. Foster, L. Golding, J. Hsu, A. Le Noac'h, H. Li, K. McDonell, N. Muennighoff, C. Ociepa, J. Phang, L. Reynolds, H. Schoelkopf, A. Skowron, L. Sutawika, E. Tang, A. Thite, B. Wang, K. Wang, and A. Zou. The language model evaluation harness, 07 2024.

- [13] A. Grattafiori, A. Dubey, A. Jauhri, A. Pandey, A. Kadian, A. Al-Dahle, A. Letman, A. Mathur, A. Schelten, A. Vaughan, et al. The llama 3 herd of models. *arXiv preprint arXiv:2407.21783*, 2024.
- [14] A. Han, J. Li, W. Huang, M. Hong, A. Takeda, P. Jawanpuria, and B. Mishra. Sltrain: a sparse plus low-rank approach for parameter and memory efficient pretraining. arXiv preprint arXiv:2406.02214, 2024.
- [15] Y. Hao, Y. Cao, and L. Mou. Flora: Low-rank adapters are secretly gradient compressors. *arXiv preprint* arXiv:2402.03293, 2024.
- [16] S. Hayou, N. Ghosh, and B. Yu. Lora+: Efficient low rank adaptation of large models. *arXiv preprint* arXiv:2402.12354, 2024.
- [17] Y. He, P. Li, Y. Hu, C. Chen, and K. Yuan. Subspace optimization for large language models with convergence guarantees. *arXiv preprint arXiv:2410.11289*, 2024.
- [18] D. Hendrycks, C. Burns, S. Basart, A. Zou, M. Mazeika, D. Song, and J. Steinhardt. Measuring massive multitask language understanding. *Proceedings of the International Conference on Learning Representa*tions (ICLR), 2021.
- [19] D. Hendrycks and K. Gimpel. Gaussian error linear units (gelus). arXiv preprint arXiv:1606.08415, 2016.
- [20] J. Hoffmann, S. Borgeaud, A. Mensch, E. Buchatskaya, T. Cai, E. Rutherford, D. d. L. Casas, L. A. Hendricks, J. Welbl, A. Clark, et al. Training compute-optimal large language models. arXiv preprint arXiv:2203.15556, 2022.
- [21] E. J. Hu, Y. Shen, P. Wallis, Z. Allen-Zhu, Y. Li, S. Wang, L. Wang, W. Chen, et al. Lora: Low-rank adaptation of large language models. *ICLR*, 1(2):3, 2022.
- [22] A. Q. Jiang, A. Sablayrolles, A. Roux, A. Mensch, B. Savary, C. Bamford, D. S. Chaplot, D. de las Casas, E. B. Hanna, F. Bressand, G. Lengyel, G. Bour, G. Lample, L. R. Lavaud, L. Saulnier, M.-A. Lachaux, P. Stock, S. Subramanian, S. Yang, S. Antoniak, T. L. Scao, T. Gervet, T. Lavril, T. Wang, T. Lacroix, and W. E. Sayed. Mixtral of experts, 2024.
- [23] Z. Jiang, X. Chen, X. Huang, X. Du, D. Zhou, and Z. Wang. Back razor: Memory-efficient transfer learning by self-sparsified backpropagation. Advances in neural information processing systems, 35:29248–29261, 2022.
- [24] S. R. Kamalakara, A. Locatelli, B. Venkitesh, J. Ba, Y. Gal, and A. N. Gomez. Exploring low rank training of deep neural networks. *arXiv preprint arXiv:2209.13569*, 2022.
- [25] J. Kaplan, S. McCandlish, T. Henighan, T. B. Brown, B. Chess, R. Child, S. Gray, A. Radford, J. Wu, and D. Amodei. Scaling laws for neural language models. arXiv preprint arXiv:2001.08361, 2020.
- [26] D. Lee, J.-Y. Lee, G. Zhang, M. Tiwari, and A. Mirhoseini. Cats: Contextually-aware thresholding for sparsity in large language models, 2024.
- [27] V. Lialin, N. Shivagunde, S. Muckatira, and A. Rumshisky. Relora: High-rank training through low-rank updates. *arXiv preprint arXiv:2307.05695*, 2023.
- [28] J. Lin, J. Tang, H. Tang, S. Yang, W.-M. Chen, W.-C. Wang, G. Xiao, X. Dang, C. Gan, and S. Han. Awq: Activation-aware weight quantization for on-device llm compression and acceleration. *Proceedings of Machine Learning and Systems*, 6:87–100, 2024.
- [29] S. Lin, J. Hilton, and O. Evans. Truthfulqa: Measuring how models mimic human falsehoods, 2022.
- [30] J. Liu, P. Ponnusamy, T. Cai, H. Guo, Y. Kim, and B. Athiwaratkun. Training-free activation sparsity in large language models, 2024.
- [31] S.-Y. Liu, C.-Y. Wang, H. Yin, P. Molchanov, Y.-C. F. Wang, K.-T. Cheng, and M.-H. Chen. Dora: Weight-decomposed low-rank adaptation. In *Forty-first International Conference on Machine Learning*, 2024.
- [32] Z. Liu, J. Wang, T. Dao, T. Zhou, B. Yuan, Z. Song, A. Shrivastava, C. Zhang, Y. Tian, C. Re, et al. Deja vu: Contextual sparsity for efficient llms at inference time. In *International Conference on Machine Learning*, pages 22137–22176. PMLR, 2023.
- [33] I. Loshchilov and F. Hutter. Decoupled weight decay regularization, 2019.

- [34] G. Malinovsky, U. Michieli, H. A. A. K. Hammoud, T. Ceritli, H. Elesedy, M. Ozay, and P. Richtárik. Randomized asymmetric chain of lora: The first meaningful theoretical framework for low-rank adaptation. arXiv preprint arXiv:2410.08305, 2024.
- [35] P. Micikevicius, S. Narang, J. Alben, G. Diamos, E. Elsen, D. Garcia, B. Ginsburg, M. Houston, O. Kuchaiev, G. Venkatesh, et al. Mixed precision training. *arXiv* preprint *arXiv*:1710.03740, 2017.
- [36] R. Miles, P. Reddy, I. Elezi, and J. Deng. Velora: Memory efficient training using rank-1 sub-token projections. In *The Thirty-eighth Annual Conference on Neural Information Processing Systems*.
- [37] I. Mirzadeh, K. Alizadeh, S. Mehta, C. C. Del Mundo, O. Tuzel, G. Samei, M. Rastegari, and M. Farajtabar. Relu strikes back: Exploiting activation sparsity in large language models. *arXiv preprint arXiv:2310.04564*, 2023.
- [38] A. Panferov, J. Chen, S. Tabesh, R. L. Castro, M. Nikdan, and D. Alistarh. Quest: Stable training of Ilms with 1-bit weights and activations. *arXiv preprint arXiv:2502.05003*, 2025.
- [39] J. W. Rae, S. Borgeaud, T. Cai, K. Millican, J. Hoffmann, F. Song, J. Aslanides, S. Henderson, R. Ring, S. Young, et al. Scaling language models: Methods, analysis & insights from training gopher. arXiv preprint arXiv:2112.11446, 2021.
- [40] C. Raffel, N. Shazeer, A. Roberts, K. Lee, S. Narang, M. Matena, Y. Zhou, W. Li, and P. J. Liu. Exploring the limits of transfer learning with a unified text-to-text transformer. *Journal of machine learning research*, 21(140):1–67, 2020.
- [41] M. A. Raihan and T. Aamodt. Sparse weight activation training. Advances in Neural Information Processing Systems, 33:15625–15638, 2020.
- [42] Rapidsai. Rapidsai/raft: Raft contains fundamental widely-used algorithms and primitives for data science, graph and machine learning., 2022.
- [43] J. Ren, S. Rajbhandari, R. Y. Aminabadi, O. Ruwase, S. Yang, M. Zhang, D. Li, and Y. He. {Zero-offload}: Democratizing {billion-scale} model training. In 2021 USENIX Annual Technical Conference (USENIX ATC 21), pages 551–564, 2021.
- [44] T. Robert, M. Safaryan, I.-V. Modoranu, and D. Alistarh. Ldadam: Adaptive optimization from low-dimensional gradient statistics. arXiv preprint arXiv:2410.16103, 2024.
- [45] J. Shah, G. Bikshandi, Y. Zhang, V. Thakkar, P. Ramani, and T. Dao. Flashattention-3: Fast and accurate attention with asynchrony and low-precision. Advances in Neural Information Processing Systems, 37:68658–68685, 2024.
- [46] N. Shazeer. Glu variants improve transformer. arXiv preprint arXiv:2002.05202, 2020.
- [47] N. Shazeer and M. Stern. Adafactor: Adaptive learning rates with sublinear memory cost. In *International Conference on Machine Learning*, pages 4596–4604. PMLR, 2018.
- [48] Y. Song, H. Xie, Z. Zhang, B. Wen, L. Ma, Z. Mi, and H. Chen. Turbo sparse: Achieving llm sota performance with minimal activated parameters. *arXiv preprint arXiv:2406.05955*, 2024.
- [49] J. Tang, Y. Zhao, K. Zhu, G. Xiao, B. Kasikci, and S. Han. Quest: Query-aware sparsity for efficient long-context llm inference. *arXiv preprint arXiv:2406.10774*, 2024.
- [50] H. Touvron, L. Martin, K. Stone, P. Albert, A. Almahairi, Y. Babaei, N. Bashlykov, S. Batra, P. Bhargava, S. Bhosale, et al. Llama 2: Open foundation and fine-tuned chat models. arXiv preprint arXiv:2307.09288, 2023.
- [51] H. Wang, S. Ma, L. Dong, S. Huang, H. Wang, L. Ma, F. Yang, R. Wang, Y. Wu, and F. Wei. Bitnet: Scaling 1-bit transformers for large language models. *arXiv preprint arXiv:2310.11453*, 2023.
- [52] H. Wang, S. Ma, R. Wang, and F. Wei. Q-sparse: All large language models can be fully sparsely-activated. arXiv preprint arXiv:2407.10969, 2024.
- [53] W. Xia, C. Qin, and E. Hazan. Chain of lora: Efficient fine-tuning of language models via residual learning. arXiv preprint arXiv:2401.04151, 2024.
- [54] G. Xiao, Y. Tian, B. Chen, S. Han, and M. Lewis. Efficient streaming language models with attention sinks. arXiv preprint arXiv:2309.17453, 2023.

- [55] A. Yang, A. Li, B. Yang, B. Zhang, B. Hui, B. Zheng, B. Yu, C. Gao, C. Huang, C. Lv, et al. Qwen3 technical report. arXiv preprint arXiv:2505.09388, 2025.
- [56] H. Zhang, Y. Zhou, Y. Xue, Y. Liu, and J. Huang. G10: Enabling an efficient unified gpu memory and storage architecture with smart tensor migrations. In *Proceedings of the 56th Annual IEEE/ACM International Symposium on Microarchitecture*, pages 395–410, 2023.
- [57] Y. Zhang, C. Chen, Z. Li, T. Ding, C. Wu, D. P. Kingma, Y. Ye, Z.-Q. Luo, and R. Sun. Adam-mini: Use fewer learning rates to gain more. *arXiv preprint arXiv:2406.16793*, 2024.
- [58] Z. Zhang, Y. Lin, Z. Liu, P. Li, M. Sun, and J. Zhou. Moefication: Transformer feed-forward layers are mixtures of experts. In *Findings of the Association for Computational Linguistics: ACL 2022*, pages 877–890, 2022.
- [59] Z. Zhang, Y. Sheng, T. Zhou, T. Chen, L. Zheng, R. Cai, Z. Song, Y. Tian, C. Ré, C. Barrett, et al. H2o: Heavy-hitter oracle for efficient generative inference of large language models. *Advances in Neural Information Processing Systems*, 36:34661–34710, 2023.
- [60] Z. Zhang, C. Xiao, Q. Qin, Y. Lin, Z. Zeng, X. Han, Z. Liu, R. Xie, M. Sun, and J. Zhou. Exploring the benefit of activation sparsity in pre-training. arXiv preprint arXiv:2410.03440, 2024.
- [61] J. Zhao, Z. Zhang, B. Chen, Z. Wang, A. Anandkumar, and Y. Tian. Galore: Memory-efficient llm training by gradient low-rank projection. arXiv preprint arXiv:2403.03507, 2024.
- [62] H. Zhu, Z. Zhang, W. Cong, X. Liu, S. Park, V. Chandra, B. Long, D. Z. Pan, Z. Wang, and J. Lee. Apollo: Sgd-like memory, adamw-level performance. *arXiv preprint arXiv:2412.05270*, 2024.
- [63] T. Zhu, X. Qu, D. Dong, J. Ruan, J. Tong, C. He, and Y. Cheng. Llama-moe: Building mixture-of-experts from llama with continual pre-training. *arXiv* preprint arXiv:2406.16554, 2024.

More Related Works

Optimizer-efficient approaches. An alternative strategy for reducing memory usage focuses on compressing optimizer states while retaining the full set of trainable parameters. GaLore [61] achieves this by projecting the gradient matrix onto a low-dimensional subspace and using the compressed gradient to compute both first- and second-order moments. Although the projection matrix is typically obtained via Singular Value Decomposition (SVD) of the true gradient [61], several more computationally efficient alternatives have been proposed, including random projections [17, 15]. norm-based scaling [6], and error feedback [44]. Another line of research aims to reduce redundancy in the optimizer states of Adam. For example, Adam-mini [57] compresses the second-order momentum, while Apollo [62] eliminates all optimizer states by using approximate gradient scaling.

Parameter-efficient approaches. A promising direction for memory-efficient training involves parameter-efficient approaches, which reduce the number of trainable parameters and, consequently, the memory overhead associated with storing optimizer states. For example, LoRA [21] and its variants [31, 16, 34] constrain updates to a low-rank subspace of each weight matrix. While these methods significantly reduce memory consumption, the limited number of trainable parameters can sometimes lead to degraded model performance [3]. To address this issue, recent work proposes employing multiple LoRA modules to enable effectively high-rank updates [27, 53]. However, in pre-training settings, this strategy still relies on an initial full-rank training phase as a warm-up before transitioning to low-rank updates [27], thereby limiting its overall memory efficiency.

B **Proof of Theorem 1**

In this section, we provide the detailed proof of Theorem 1.

Proof of Theorem 1. Given $a \leq b$ and $d_{\mathrm{ffn}} \in \mathbb{N}^*$, it suffices to prove that for $\forall f \in \mathcal{H}_{d_{\mathrm{ffn}}}$, we have $f \in \mathcal{H}_{d_{\mathrm{moc}}}^{a:b}$, where $d_{\mathrm{moc}} = b \lceil d_{\mathrm{ffn}}/a \rceil$. According to the definition of $\mathcal{H}_{d_{\mathrm{ffn}}}$, there exist weight matrices $W_{\mathrm{gate}}, W_{\mathrm{up}} \in \mathbb{R}^{d \times d_{\mathrm{ffn}}}$ and $W_{\mathrm{down}} \in \mathbb{R}^{d_{\mathrm{ffn}} \times d}$ such that f can be parameterized as $f = \mathrm{FFN}(W_{\mathrm{gate}}, W_{\mathrm{up}}, W_{\mathrm{down}})$. Let $k = \lceil d_{\mathrm{ffn}}/a \rceil$ and $r = ka - d_{\mathrm{ffn}}$, it holds that $0 \le r < a$ and $d_{\mathrm{moc}} = kb$. We construct matrices $W'_{\mathrm{gate}}, W'_{\mathrm{up}} \in \mathbb{R}^{d \times d_{\mathrm{moc}}}$ and $W'_{\mathrm{down}} \in \mathbb{R}^{d_{\mathrm{moc}} \times d}$ as follows:

$$\begin{aligned} & W_{\text{gate}}^{\prime}[i,j] = \begin{cases} W_{\text{gate}}[i,k'a+r'+1], & \text{if } j-1=k'b+r', \ k',r'\in\mathbb{N}, \ r'< a, \ k'a+r'< d_{\text{ffn}}; \\ 0, & \text{otherwise}; \end{cases} \\ & W_{\text{up}}^{\prime}[i,j] = \begin{cases} W_{\text{up}}[i,k'a+r'+1], & \text{if } j-1=k'b+r', \ k',r'\in\mathbb{N}, \ r'< a, \ k'a+r'< d_{\text{ffn}}; \\ 0, & \text{otherwise}; \end{cases} \\ & W_{\text{down}}^{\prime}[i,j] = \begin{cases} W_{\text{gate}}[k'a+r'+1,j], & \text{if } i-1=k'b+r', \ k',r'\in\mathbb{N}, \ r'< a, \ k'a+r'< d_{\text{ffn}}; \\ 0, & \text{otherwise}; \end{cases} \\ & W_{\text{down}}^{\prime}[i,j] = \begin{cases} W_{\text{gate}}[k'a+r'+1,j], & \text{if } i-1=k'b+r', \ k',r'\in\mathbb{N}, \ r'< a, \ k'a+r'< d_{\text{ffn}}; \\ 0, & \text{otherwise}; \end{cases} \end{aligned}$$

$$W_{\text{up}}'[i,j] = \begin{cases} W_{\text{up}}[i,k'a+r'+1], & \text{if } j-1=k'b+r', \ k',r' \in \mathbb{N}, \ r' < a, \ k'a+r' < d_{\text{ffn}}; \\ 0, & \text{otherwise}; \end{cases}$$

$$W'_{\text{down}}[i,j] = \begin{cases} W_{\text{gate}}[k'a + r' + 1, j], & \text{if } i - 1 = k'b + r', \ k', r' \in \mathbb{N}, \ r' < a, \ k'a + r' < d_{\text{ffin}}; \\ 0, & \text{otherwise}; \end{cases}$$

Consider $f' = \text{MoC}_{a:b}(W'_{\text{gate}}, W'_{\text{up}}, W'_{\text{down}}) \in \mathcal{H}^{a:b}_{d_{\text{moc}}}$, we show that f'(x) = f(x) for any d-dimensional row vector x. We define $g = xW_{\text{gate}}, u = xW_{\text{up}}, s = \text{SiLU}(g), z = s \odot u$ such that $f(x) = zW_{\text{down}}$, and define $g' = xW'_{\text{gate}}, u' = xW'_{\text{up}}, s' = \text{SiLU}(g'), s'' = \text{TopK}_{a:b}(s')$, and $z' = s'' \odot u'$ such that $f'(x) = z'W'_{\text{down}}$. Here, $\text{TopK}_{a:b}$ preserves the a entries with the largest absolute values in every consecutive block of b entries and sets the rest to zero. For an input vector $x \in \mathbb{R}^{mb}$, this means that for $k' = 0, 1, \dots, m-1$ and $r' = 1, 2, \dots, b$:

TopKa:
$$b(x)[k'b+r']$$

$$=\begin{cases} x[k'b+r'], & \text{if } |x[k'b+r']| \text{ is among the top-}a \text{ in } |x[k'b+1]|, \dots, |x[k'b+b]|, \\ 0, & \text{otherwise.} \end{cases}$$

According to the definition of W'_{gate} , we have

$$\begin{split} g'[j] = & x W_{\text{gate}}'[:,j] \\ &= \begin{cases} x W_{\text{gate}}[:,k'a+r'+1], & \text{if } j-1=k'b+r', \ k',r' \in \mathbb{N}, \ r' < a, \ k'a+r' < d_{\text{ffn}}; \\ 0, & \text{otherwise}; \end{cases} \\ &= \begin{cases} g[k'a+r'+1], & \text{if } j-1=k'b+r', \ k',r' \in \mathbb{N}, \ r' < a, \ k'a+r' < d_{\text{ffn}}; \\ 0, & \text{otherwise}; \end{cases} \end{split}$$

Similarly, we have

$$u'[j] = \begin{cases} u[k'a + r' + 1], & \text{if } j - 1 = k'b + r', \ k', r' \in \mathbb{N}, \ r' < a, \ k'a + r' < d_{\text{ffn}}; \\ 0, & \text{otherwise}; \end{cases}$$

thus

$$\begin{split} s'[j] = & \text{SiLU}(g'[j]) \\ = & \begin{cases} & \text{SiLU}(g[k'a + r' + 1]), & \text{if } j - 1 = k'b + r', \ k', r' \in \mathbb{N}, \ r' < a, \ k'a + r' < d_{\text{ffn}}; \\ & 0, & \text{otherwise}; \end{cases} \\ = & \begin{cases} & s[k'a + r' + 1], & \text{if } j - 1 = k'b + r', \ k', r' \in \mathbb{N}, \ r' < a, \ k'a + r' < d_{\text{ffn}}; \\ & 0, & \text{otherwise}; \end{cases} \end{split}$$

Noting that for $\forall k' \in \{0, 1, \cdots, k-1\}$, there are at least (b-a) zero elements s'[k'b+a+1], $s'[k'b+a+2], \cdots, s'[k'b+b]$ in the b consecutive terms from s'[k'b+1] to s'[k'b+b], we have s''=s' since all non-zero elements of s' is maintained in the TopK $_{a:b}$ selection. This indicates

$$\begin{split} &z'[j] = s''[j] \cdot u'[j] = s'[j] \cdot u'[j] \\ &= \begin{cases} s[k'a + r' + 1] \cdot u[k'a + r' + 1], & \text{if } j - 1 = k'b + r', \ k', r' \in \mathbb{N}, \ r' < a, \ k'a + r' < d_{\text{ffn}}; \\ 0, & \text{otherwise}; \end{cases} \\ &= \begin{cases} z[k'a + r' + 1], & \text{if } j - 1 = k'b + r', \ k', r' \in \mathbb{N}, \ r' < a, \ k'a + r' < d_{\text{ffn}}; \\ 0, & \text{otherwise}; \end{cases} \end{split}$$

Consequently, we have

$$\begin{split} f'(x)[j] &= \sum_{i=1}^{d_{\text{moc}}} z'[i] \cdot W'_{\text{down}}[i,j] \\ &= \sum_{\substack{k',r' \in \mathbb{N}, r' < a \\ k'a+r' < d_{\text{ffn}}}} z[k'a+r'+1] \cdot W_{\text{down}}[k'a+r'+1,j] \\ &= \sum_{i=1}^{d_{\text{ffn}}} z[i] \cdot W_{\text{down}}[i,j] = f(x)[j], \end{split}$$

which implies f(x) = f'(x). By the arbitrariness of x, we conclude that $f = f' \in \mathcal{H}^{a:b}_{d_{\text{moc}}}$, which completes the proof.

Remark. The Top-*K* strategy used in the proof of Theorem 1 slightly differs from that described in Section 3.2. The proof selects entries with the largest absolute values of the SiLU outputs, whereas Section 3.2 adopts a more efficient approximation by selecting the top (non-absolute) values of the SiLU inputs. Since SiLU activations for negative inputs are close to zero, selecting top SiLU inputs serves as a good approximation to selecting the top absolute values of the outputs. We adopt this input-based selection in practice for improved computational efficiency.

C Pre-training Experimental Details

C.1 Experimental Setup

Table 19: Detailed configurations in each pre-training experiment.

Params	Hidden	Intermediate	Heads	Layers	Training Tokens	Learning Rate
60M	512	1376	8	8	1.3B	2.5E-3
130M	768	2048	12	12	2.6B	2.5E-3
350M	1024	2736	16	24	7.8B	1E-3
1B	2048	5461	24	32	13.1B	6E-4

Table 20: Detailed configurations in pre-training experiments of Mixtral.

Params	Experts	Hidden	Intermediate	Heads	Layers	Training Tokens	Learning Rate
180M	2/8	512	1376	8	8	2.6B	2.5E-3
530M	2/8	768	2048	12	12	7.8B	1E-3

For LLaMA pre-training across all model sizes, we follow the setup outlined in [61, 14]. We use a total batch size of 512 and a maximum sequence length of 256, resulting in approximately 131K tokens per batch. The AdamW optimizer is employed with momentum parameters $(\beta_1, \beta_2) = (0.9, 0.999)$ across all experiments. The learning rate follows a cosine annealing schedule, preceded by linear warm-up during the first 10% of training steps. Weight decay is set to 0. Detailed configurations and hyperparameters for each experiment are provided in Table 19.

C.2 Training Efficiency

We evaluate the training throughput of different methods by pre-training LLaMA-350M and LLaMA-1B with batch sizes of 128 and 64, respectively, on a single NVIDIA A800 GPU. Throughput is measured in tokens processed per second and averaged over 1,000 training steps. As shown in Table 9, MoC achieves training efficiency comparable to the vanilla LLaMA model.